Desalination and Water Treatment
www.deswater.com

doi: 10.5004/dwt.2021.27459

231 (2021) 152–165
August

A facile approach to fabricate metal coordinated carboxylated alginic acid-based adsorbent for efficient removal of chromium(VI)

Khalid A. Alamry[a,*], Raed H. Althomali[a], Ajahar Khan[a], Abeer M. Alosaimi[b], Mahmoud A. Hussein[a,c,*]

[a]*Department of Chemistry, Faculty of Science, King Abdulaziz University, Jeddah 21589, Saudi Arabia, emails: kaalamri@kau.edu.sa (K.A. Alamry), mahussein74@yahoo.com/maabdo@kau.edu.sa (M.A. Hussein), r.h-t@hotmail.com (R.H. Althomali), arkhan.029@gmail.com (A. Khan)*
[b]*Department of Chemistry, Faculty of Science, Taif University, P.O. Box: 11099, Taif 21944, Saudi Arabia, email: abeer_alosaimi@hotmail.com*
[c]*Polymer Chemistry Lab, Chemistry Department, Faculty of Science, Assiut University, Assiut 71516, Egypt*

Received 10 December 2020; Accepted 5 May 2021

ABSTRACT

Metal carboxylated alginic acid (M-CAA) based adsorbents were prepared for the efficient removal of Cr(VI) from an aqueous solution. Batch mode adsorption studies were carried out by varying temperature, pH, initial Cr(VI) concentration, and shaking time. The fabricated adsorbents were characterized by field emission scanning electron microscopy, energy dispersive X-ray, X-ray diffraction, and Fourier transform infrared spectroscopy. Moreover, the pseudo-first-order, pseudo-second-order, Elovich, and fractional power adsorption Kinetic were applied to models in the adsorption data. The kinetics of a reaction followed the pseudo-second-order model and intra-particle diffusion pattern. The thermodynamic verified that the Cr(VI) sorption of Zr-CAA was spontaneous and endothermic. The chromium sorption capacity of fabricated Zr-CAA adsorbent material was achieved at 7.14 mg g^{-1} at pH 1.

Keywords: Spectrophotometric analysis; Carboxylated alginic acid; Solid phase extraction; Metal coordinate; Environmental effects

1. Introduction

Since the last few decades, contaminated water has been a major concern of developed countries due to the release of industrial and domestic wastes into water bodies [1]. Water is mainly contaminated by chemical and biological waste that causes adverse effects on the lives of most living organisms, becoming responsible for many serious diseases. Water contamination caused by industrial wastes possesses toxic heavy metals like copper, lead, chromium, zinc, cadmium, and nickel [2]. Among these, chromium is considered to be a more toxic and naturally occurring metal that can be found in soil, water, and air. Chromium available in natural water is generally precipitated as chromium hydroxide having minimized solubility [3]. Furthermore, chromium is mainly present as trivalent chromium (Cr(III)), which is converted into hexavalent chromium (Cr(VI)) during industrial processes via the oxidation of Cr(III), which is produced as industrial waste. This Cr(VI) is highly toxic compared to any other type of Cr and responsible for causing many serious diseases such as liver damage, cancer, reducing reproductive health, atrapat genetic, and inflammation of the skin, and severe diarrhea [3,4]. It can easily reach the bloodstream and exhibit toxic effects. A higher concentration of chromium above the permissible limit, as suggested by the World Health Organization (WHO), in the aqueous system causes various life-threatening diseases [5]. Further, the United States Environmental Protection Agency (EPA) states that the standard amount of chromium in drinking water should not be more than 0.1 mg L^{-1} or 100 ppb for total chromium (includes all forms of chromium) [6].

* Corresponding authors.

Conventional methods used for the removal of toxic Cr(VI) include many techniques such as chemical oxidation, catalysis, electrochemical treatment, liquid–liquid extraction, reverse osmosis, macro-scales, and coagulation, [1,7] adsorption [8], membrane filtration [9], ion exchange [10], precipitation, [11], and nanofiltration [12], etc. Among them, adsorption is being used extensively for removing heavy metals from the aqueous solution; the usefulness of this method lies in the benefits of a cleaner and easily controlled process, availability, high-efficiency, and more efficient and cost-effective technology; many adsorbents have been reported for the adsorption of Cr(VI) from aqueous phase [3], such as α-Fe_2O_3 [13] mesoporous TiO_2, [14] activated carbon [15], etc. However, the efficiency capacity of these materials is less than required; all materials are limited when used for Cr(VI) removal. As a result, there is an urgent need to improve new adsorbents with high surface areas and large adsorption capacities.

The literature review suggested that the extraction of heavy metals needs several chemicals and some sophisticated instruments, which makes it more difficult, expensive, and time-consuming. Moreover, biosorption is an important technique for wastewater treatment due to its feasibility, eco-friendliness, and low operation cost [16]. Bio-polymers are considered to be more interested in the day-to-day environment that can treat water in a safe, easy, and detoxicated manner at a low cost. It has been reported that several biopolymers including cellulose, chitin, and hemicellulose have already been tried for the removal of chromium(VI) and other toxic heavy metals from aqueous media [17–21].

Presently, scientists are paying increased attention to the development of biopolymers such as cellulose, chitosan, alginate, and chitin-based composite materials that can be used for the application of wastewater treatment [22]. Polysaccharides such as alginic acid (AA), which is characterized by its vitality and nontoxicity, consist of functional groups such as hydroxyl and carbonyl groups active on the rings. This polysaccharide is biocompatible, biodegradable, and hemocompatible; it has not been found to accumulate in biological systems [23]. Therefore, AA could be used for several applications because of its inert behavior. With the rapid growth in the field of material science, many inorganic and organic nanocomposite materials are synthesized through the control of matter and verified for desirable functional properties [24].

Herein, we introduced the fabrication of carboxylated alginic acid (CAA) coordinated with Zr(IV) (Zr-CAA) and Ni(II) (Ni-CAA) for the removal of toxic chromate from the aqueous phase. Firstly, alginic acid (AA) was chemically oxidized via potassium permanganate to give CAA. This modified CAA was coordinated with high valence metal ion (Ni^{2+}) and (Zr^{4+}) through a simple chemical route. Therefore, to confirm the fabrication of proposed materials, techniques such as X-ray powder diffraction (XRD), field emission scanning electron microscopy (FESEM), and Fourier transform infrared spectroscopy (FT-IR) were carried out. Additionally, UV-vis and solid-phase extraction were used to confirm the successful removal of Cr(VI) from aqueous solutions using different parameters such as heating, ions effect, shaking time, and pH. The thermodynamic and kinetic parameters verified that the nature of Cr(VI) removal was spontaneous and endothermic.

2. Experimental details

2.1. Reagents and materials

The following materials were used: alginic acid (AA) from BDH Chemicals Ltd., Poole, England; potassium permanganate ≥99.0%, hydrochloric acid 37%, and potassium chromate (purity 98.5%) from Aldrich Chemical Co., Ltd., Milwaukee, WC, USA; $ZrOCl_2{\cdot}8H_2O$ (purity 98.0%) and $NiCl_2{\cdot}4H_2O$ (purity 99.9%), tap water from chemical laboratory and sewage water from King Abdulaziz University; seawater from the Red Sea, Saudi Arabia. The solvents and chemicals were of analytical reagent-class, utilized without any purification.

2.2. Preparation of reagent solutions

A stock solution of chromium salt (1,000 μg mL^{-1}) in deionized water was made with potassium dichromate, which was used to prepare more diluted standard solutions (20–100 μg mL^{-1}) with deionized water. A series of buffers of pH (2–11) and HCl (0.1 mol L^{-1}) were prepared to use as an extraction medium for the removal of chromium ions by solid-phase extraction.

2.3. Instruments

All spectrophotometric determinations were carried out with a UV-visible spectrophotometer (Perkin-Elmer, USA). The stock solutions of chromium ions were made by a digital micropipette (Volac); a pH meter (Orion-model EA 940) was used to measure the pH of the prepared solutions. An electronic analytical weighing balance (0.0001 g) from Sartorius, Germany; magnetic stirrer with hotplate 16 cm × 16 cm, Digital, SD160 from Stuart equipment company; Corporation Precision Scientific mechanical shaker (Chicago, CH, USA) with a shaking rate in the range of 10–250 rpm were used during sample preparation. To obtain deionized water, the Milli-Q Plus system (Millipore, Bedford, MA, USA) was employed. FESEM micro-images for the fabricated materials were obtained using a Quanta 600 FEG scanning electron microscopy (SEM) from FEI Company, USA. The XRD pattern was recorded using Bruker (Germany) DMAX 2500and FT-IR Perkin Elmer Spectrum, USA (RX1 FT-IR (Range: 500–4,000 cm^{-1})).

2.4. Preparation of coordinated Zr-CAA and Ni–CAA

In a typical procedure, the oxidation of alginic acid (5 g) was carried out using potassium permanganate (10 mM) as an oxidizing agent under strong mechanical agitation at 30° up to 30 min. It was reported that the use of potassium permanganate within the range of 10 mM is very dangerous due to its explosive nature [16]. Now, the solution mixture was allowed to centrifuge to get CAA followed by washing with deionized water till the pH reached the range of 6–7. Subsequently, CAA was kept in the oven at 60°C for 2 h for the evaporation of solvents.

Following the above, the prepared CAA was used to coordinate with Zr^{+4} and Ni^{+2} metals. For this, CAA was taken into two round bottom flasks (each containing 2 g in 100 mL of deionized water followed by the addition of 0.2 mol L^{-1} of $ZrOCl_2 \cdot 8H_2O$ and $NiCl_2 \cdot 4H_2O$ with constant stirring for 24 h at room temperature. The pH of both the solution mixtures was adjusted to ~4 using aqueous solutions of (1 M) H_2SO_4 and NaOH. Finally, after filtration, the final products were washed several times with deionized water and dried into the oven at 60°C for 4 h; the adsorbents were then ready for the removal of chromium(VI).

2.5. Batch extraction steps

The 10 mL of tested solution was prepared by taking chromium (20 mg L^{-1}) and HCl (0.10 mol L^{-1}) followed by the addition of M-CAA (20 mg L^{-1}) on a mechanical shaker with a shaking time of 1 h. To know the exact amount of chromium ions extracted by the fabricated metal coordinated CAA adsorbents, the number of chromium ions present in the separated aqueous phase before and after shaking was determined photometrically [25]. Different kinetic models were applied to find out the actual adsorption percentage (E%) and distribution coefficient (K_d) of adsorbed chromium(VI) ions on metal coordinated CAA adsorbents at equilibrium (per unit mass of the adsorbed chromium ions (QE) per unit mass of M-CAA (mol g^{-1}). Here, the effect of temperature and shaking time was also considered to be explained the adsorption behavior of Zr-CAA toward chromium ions. Moreover, to check the effect of interference ions, 10 mL of Mg^{+2}, Fe^{+2}, Bi^{+2}, and Pb^{+2} (40 ppm each) were mixed with 10 mL of chromium(VI) (20 ppm) followed by shaking for 1 h at room temperature.

2.6. Environmental applications and sample collection

The samples used to find out the extraction efficiency were primarily tap water from the chemical laboratory, sewage water, and seawater. All the water samples were filtered and kept at 5°C in a Teflon packaging to keep away from direct light and heat. The pH for all the three water samples containing chromium ions and metal coordinated CAA adsorbent was adjusted to 1 using 1 M HCl solution. Then, the number of chromium ions extracted was calculated to evaluate the efficiency of the fabricated adsorbents for the removal and recovery of chromium ions.

3. Results and discussion

The repulsive electrostatic interactions of Cr(VI) anionic species such as hydrochromate ($HCrO_4^-$), dichromate ($Cr_2O_7^{2-}$), or chromate (CrO_4^{2-}) are rarely adsorbed by soil particles; hence, it is essential to regulate the Cr(VI) in industrial wastes. The Cr(VI) can be removed effectively due to electrostatic interaction on the surface of Zr-CAA in an acidic medium as illustrated in Fig. 1. The UV-vis spectroscopy was executed to evaluate the influences of Zr-CAA and Ni-CAA toward the removal of Cr(VI) from the aqueous media. Fig. 2a–c shows the UV-vis spectra of Cr ions, pure AA, and Zr-CAA. This can be observed from Fig. 2a, wherein the chromium ion exhibits a maximum absorbance peak in the range of 350 nm. However, with the addition of AA and Zr-CAA, the decrease in the absorbance peaks due to Chromium around 350 nm can be seen in Fig. 2b and c. Moreover, this decrease in the absorbance peaks for chromium ions is more for Zr-CAA adsorbents compared to the AA. On the other hand, the addition of Ni-CAA did not show any significant decrease

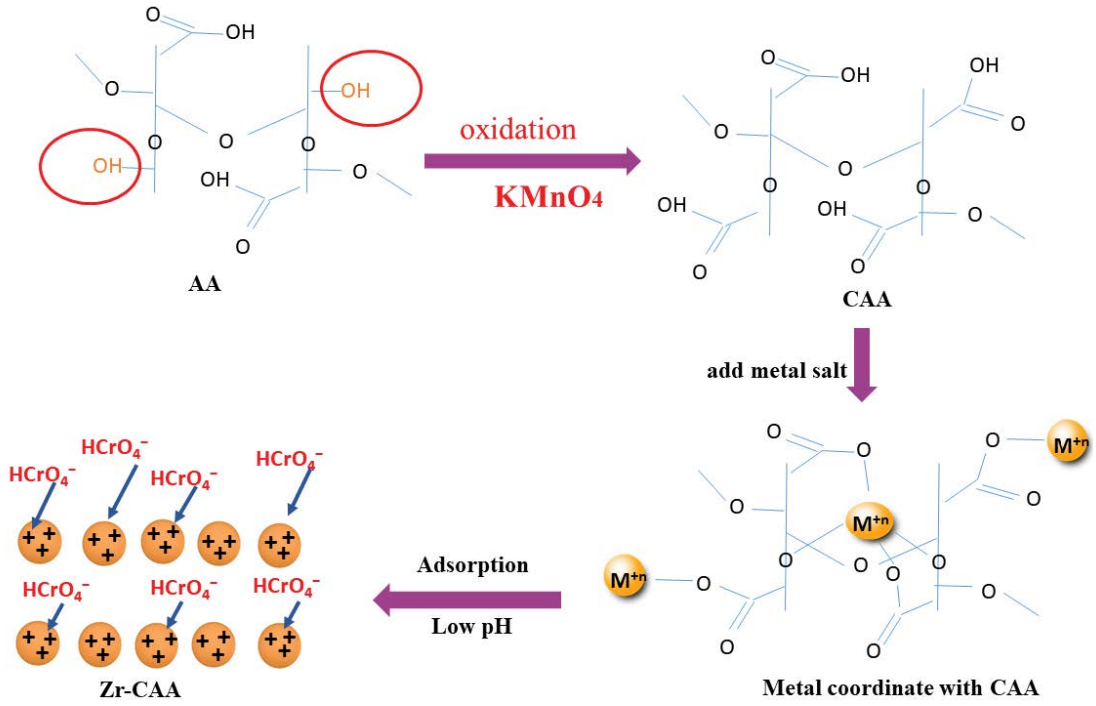

Fig. 1. Possible mechanism for the adsorption of Cr(VI) by Zr-CAA adsorbent.

in the absorbance peak appear due to chromium ions (Fig. 3c). Therefore, the results obtained from this analysis suggested that Zr-CAA was more effective toward the adsorption of chromium ions compared to Ni-CAA and AA (Fig. 3a–c). Furthermore, the coordination of CAA with Ni was not found to be suitable for the removal of chromium ions from the aqueous media. Therefore, due to the high efficiency of Zr-CAA for the removal of Cr(VI), as compared to Ni-CAA, further studies were carried out only with Zr-CAA. In addition, the adsorption of Cr(VI) on the surface of Zr-CAA was performed at lower pH because the previous literature suggested that with the decrease in the value of pH from 12 to 5, the adsorption efficiency of Cr(VI) by an adsorbent increases [26–28]. It has been reported that H_2CrO_4 and $HCrO_4^-$ mainly exist below pH = 6.8, while the CrO_4^{2-} anionic species is dominant above pH = 6.8 [29,30]. Therefore, it can be expected that considerable electrostatic attraction can emerge between Zr-CAA and the Cr(VI) anions at low pH (acidic medium). This electrostatic interaction endorses the Cr(VI) adsorption on the surface Zr-CAA adsorbent at lower solution pH.

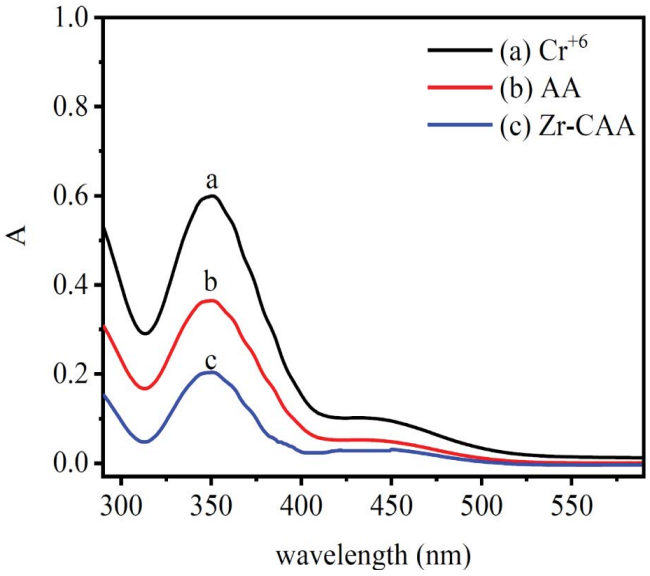

Fig. 2. Electronic spectra of chromium ions in the aqueous phase in the absence of Zr-CAA (a), after adding 25 mg of AA solid phase and shaking 1 h (b), and after adding 25 mg of Zr-CAA and shaking 1 h (c).

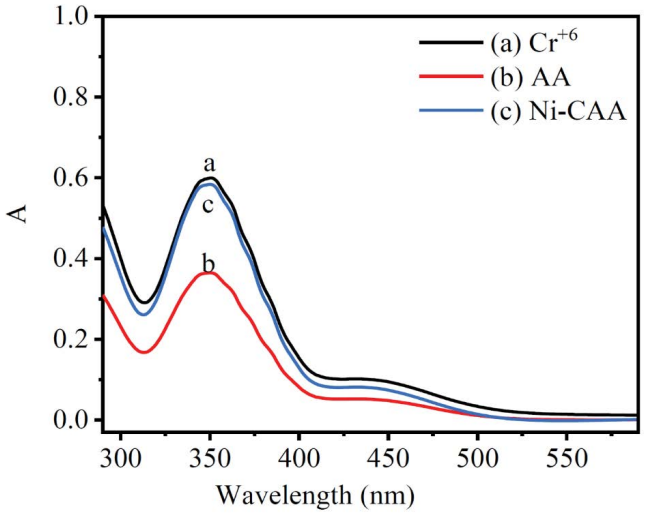

Fig. 3. Electronic spectra of chromium ions in the aqueous phase in the absence of Ni-CAA (a), after adding 25 mg of AA solid phase and shaking 1 h (b), and after adding 25 mg of Ni-CAA and shaking 1 h (c).

3.1. Characterization of Zr-CAA

3.1.1. FT-IR spectroscopy

FT-IR spectroscopy is considered to be an important tool to understand the presence of functional groups present in the prepared compound. Fig. 4 represents the FT-IR spectra for AA, CAA, pristine Zr-CAA, and Zr-CAA after adsorbing chromium ions. Fig. 4a and b clearly show the bands around 1,740 cm^{-1} attributed due to the stretching vibration of carbonyl groups present in both CAA and AA. In the case of CAA, the band around 3,000–3,600 cm^{-1} and became diminished compared to the band for alginic acid in the same region [16], which verified the conversion of carboxyl groups into carbonyl groups (Fig. 4a and b). Further, Fig. 4c shows that the band in the region 1,745 cm^{-1} (C=O stretching vibration) disappeared; the band around 3,000–3,600 cm^{-1} appeared again due to the stretching of –OH group of carboxylic acid. This verified that the protons in the carboxylic acid were replaced through metal ions [31]. In the case of Fig. 4d after chromium adsorption by Zr-CAA, the broadening and shifting of bands 3,400 and 1,582 cm^{-1} toward lower frequency region can be observed due to the electrostatic adsorption chromium by Zr-CAA [32].

3.1.2. XRD of CAA and Zr-CAA

The XRD pattern was carried out to investigate the crystal lattice structure of CAA and Zr-CAA adsorbent materials. Fig. 5 exhibits the XRD spectra of CAA and Zr-CAA.

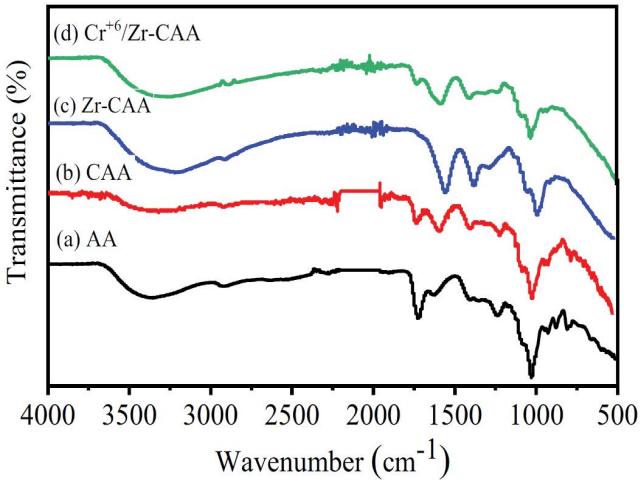

Fig. 4. FTIR spectra of (a) AA, (b) CAA, (c) Zr-CAA, and (d) chromium(VI) sorbed Zr-CAA.

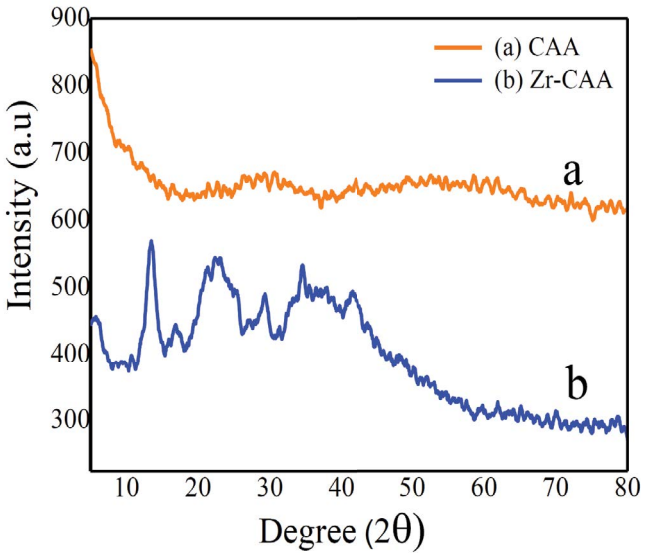

Fig. 5. XRD pattern of (a) CAA and (b) Zr-CAA.

The characteristic crystalline peaks of CAA were assigned at 14.46° and 21.30°, representing the reflection of (4 2 2) and (5 1 1) planes, respectively (Fig. 5a) [33]. Moreover, the strong diffraction pattern for Zr-CAA appeared at 29.57°, 35.43°, 50.01°, and 61.11°, representing the crystalline planes (100), (102), (130), and (120) of the Zr metal [34]. Therefore, the XRD results suggested that the characteristic and individual XRD patterns of CAA and Zr were reserved in the XRD spectra of Zr coordinated CAA adsorbent (Fig. 5b). This analysis also confirms the semi-crystalline nature, which improves the structural stability of the fabricated Zr-CAA adsorbent material.

3.1.3. Scanning electron microscopy and energy dispersive X-ray analysis

The surface morphology of the fabricated Zr-CAA adsorbent was studied by the SEM and energy dispersive X-ray (EDAX) analyses as illustrated in Fig. 6a–f. Fig. 6a–d represents the surface appearance of the proposed Zr-CAA adsorbent material at different magnifications. The digital images in Fig. 6a–d show that the surface of the Zr-CAA appeared to be rough, uneven, and porous, which might deliver appropriate binding sites for the adsorption of Cr(VI) molecules. In close view, the Zr-CAA adsorbent material surface possesses uneven and polygonal-like particles uniformly distributed with some pores and gaps (Fig. 6d). Furthermore, Fig. 6a–d shows the FE-SEM images of the surface morphologies of Zr-CAA adsorbent while Fig. 6e–f display the surface morphologies of Zr-CAA after adsorbing Cr(VI) ions. Fig. 6e–f show that a smooth Zr-CAA adsorbent surface (after adsorbing Cr(VI) ions) with well-interconnected domains leaving behind negligible space at the surface can be seen easily, while for Zr-CAA adsorbent without treating with Cr(VI), the rough, uneven, and porous nature of the surface can be observed (Fig. 6a–d). After adsorption, the Cr(VI) leads to occupying most of the accessible gaps present in the rough and uneven surface of the proposed materials that might be responsible for the higher uptake of the toxic Cr(VI) ions. Moreover, the uneven and rough surfaces of the Zr-CAA adsorbent (Fig. 6a–d) change into a slightly smooth surface with slight roughness after treating with Cr(VI) ions (Fig. 6e–d). Thus, there was very little change in the surface morphology of the Zr-CAA adsorbent material after the adsorption of Cr(VI) ions. Therefore, this negligible change in the surface morphology of the Zr-CAA adsorbent after the adsorption of Cr(VI) ions suggested that the material is stable and suitable for multiple repeats.

The elemental components of the Zr-CAA adsorbent material were investigated by EDAX analysis (Fig. 6g and h). Fig. 6g represents the surface of Zr-CAA used to analyze the major elements present in the proposed materials. In Fig. 6h, the significant elements of Zr-CAA adsorbent material such as O, C, and Zr peaks can be observed. The sharp peak of Zr in the elemental analysis suggests successful coordination of Zr metal with the CAA.

3.2. Retention profile of Cr(IV) onto AA and (Zr-CAA) in aqueous media

To evaluate the potentiality of AA and Zr-CAA adsorbent material for the removal of chromium ions, different parameters were considered in the aqueous solution. The effect of mixing volume ratios of adsorbent and adsorbate was studied at different pH, contact time, and temperatures. The experimental consequences reveal that the variation of pH and the mixing volume ratios of Zr-CAA adsorbents affect the chromium ions' adsorption in the aqueous solution. A detailed description of the above is given below. A simple illustration of the detailed fabrication steps for Zr-CAA composite material as an example for the M-CAA completes involved in this work is given in Fig. 7.

3.2.1. Effect of pH

As a significant water chemistry factor, pH can extensively affect the interactions of adsorbent and adsorbate. These parameters were decided to attain the maximum efficiency for the adsorption and recovery of chromium ions. Therefore, the effect of pH for the adsorption of chromium ions onto Zr-CAA adsorbent material was studied in the pH range 1–8 with the shaking time of 1 h. To get the maximum adsorption, the concentration of chromium(VI) present in aqueous media after equilibrium was analyzed photometrically to get the maximum adsorption [34,35]. Fig. 8 shows the adsorption behavior of chromium(IV) using Zr-CAA from the aqueous solutions. It can be clearly seen from Fig. 8 that Zr-CAA attributes maximum adsorption of chromium ions, which gradually decreased with the increase in the pH value. Further, the removal of chromium with Zr-CAA was found to be higher than that of pure AA. Moreover, the results obtained through this analysis reveal that the pH value in the range of 1–2 was suitable at which the Zr-CAA attributes maximum extraction of chromium ions from aqueous media. Therefore, further studies were carried out at pH 1.

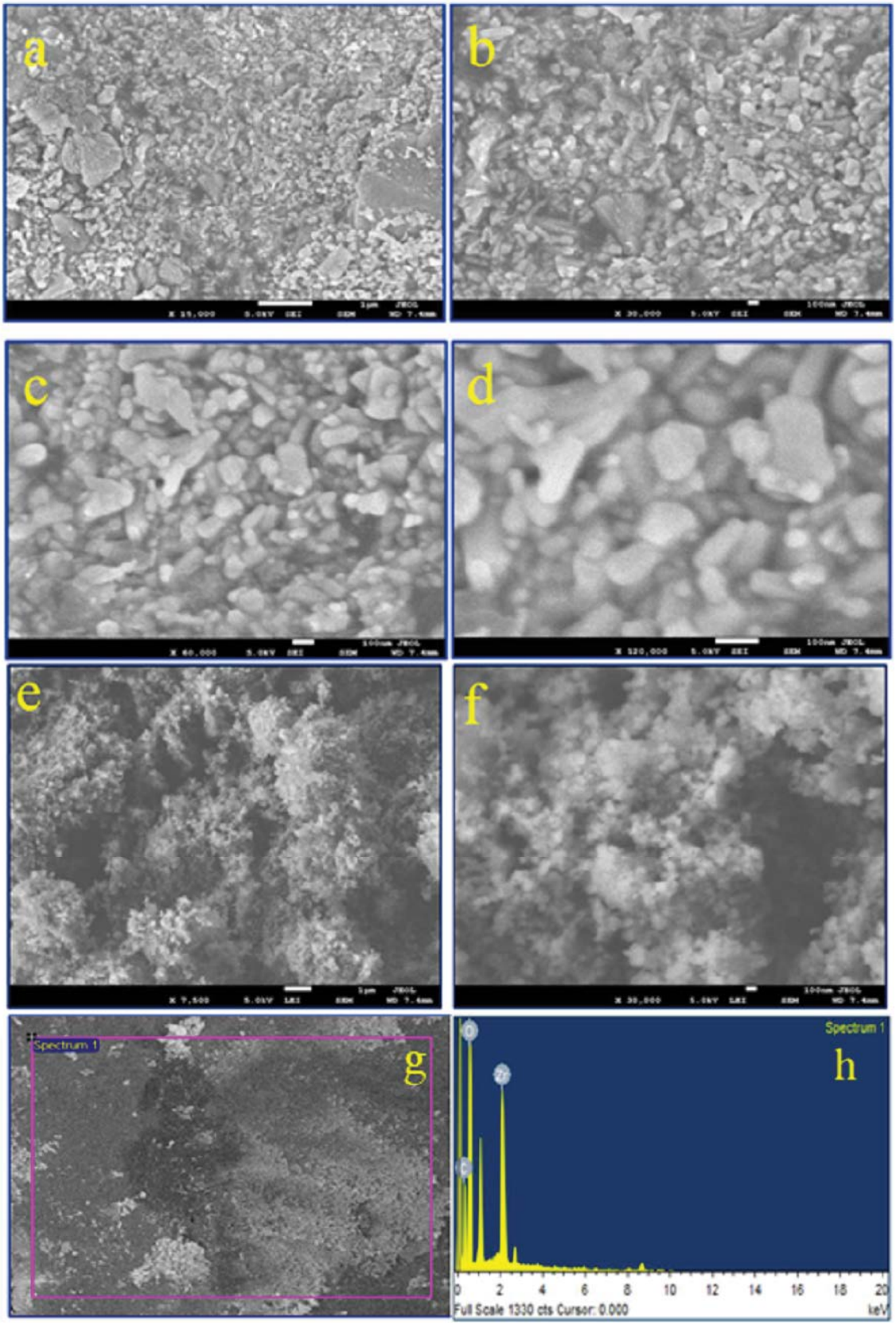

Fig. 6. (a–d) SEM micrographs of Zr-CAA at different magnifications, (e and f) Zr-CAA adsorbent after treating with Cr(VI) ions, (g) surface used for EDAX analysis, and (h) EDAX spectrum of Zr-CAA.

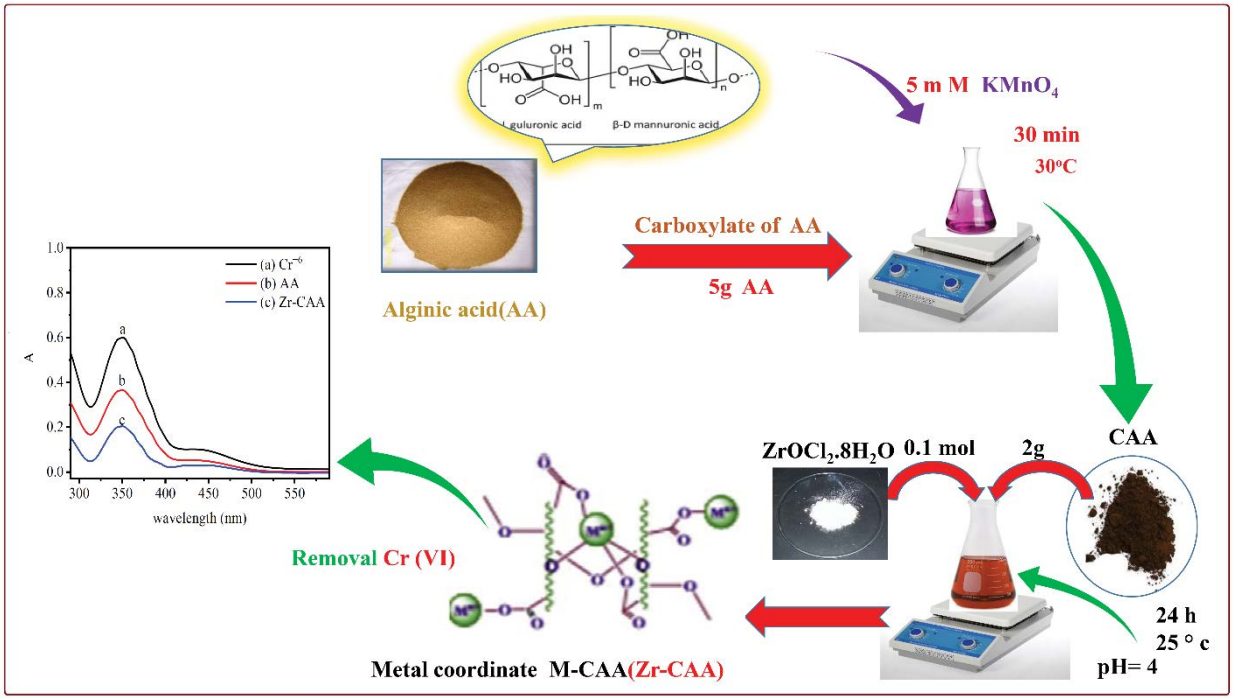

Fig. 7. Simple illustration of the detailed fabrication steps for Zr-CAA composite material.

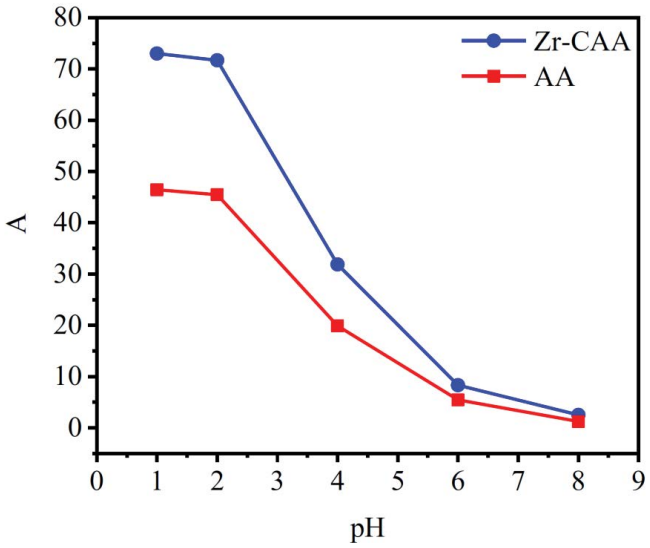

Fig. 8. Effect of the solution pH on the absorption of Cr(IV) from aqueous media onto AA and Zr-CAA (0.03 ± 0.002 g) with shaking time 1 h at 20°C ± 0.1°C.

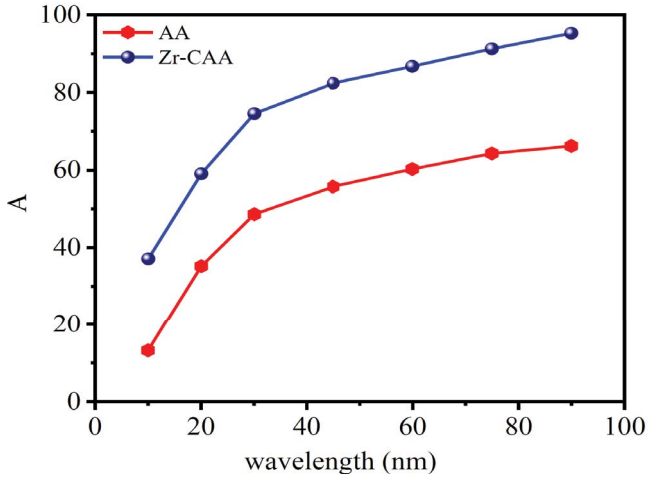

Fig. 9. Effect of Zr-CAA and AA mass on the adsorption of Cr(VI) from aqueous media at 20°C.

3.2.2. Influence of concentration

The adsorption of Cr(IV) onto Zr-CAA adsorbent material was studied by the varying concentration of AA and Zr-CAA in the range of 10–90 mg L^{-1} at pH 1 with the shaking time of 1 h. Fig. 9 represents that the percentage of chromium ions removal using AA was increased from 13% to 66%; for Zr-CAA the chromium ions, the removal was enhanced from 37% to 96%. This analysis suggested that as the mass of AA and Zr-CAA increased, the adsorption percentage of Cr(VI) from aqueous media also gradually increased. Moreover, the Zr-CAA was found to be more effective for the removal of chromium ions from the aqueous solution compared to pure AA, which may be due to the limited availability of adsorption sites on the polymer backbone of pure AA.

3.2.3. Effect of temperature and time

The adsorption of Cr(VI) on AA and Zr-CAA adsorbent materials was carried out at different contact times (5–90 min). The contact time between adsorbent and adsorbate is one of the most influencing parameters affecting

the removal of pollutants from the aqueous environment through adsorption. The influence of contact time on the removal of chromium ions by Zr-CAA and AA was studied as shown in Fig. 10. It can be seen that the increase in the contact time led to the increase of the adsorption process. This effect was especially observed within the first 45 min where most chromium ions were adsorbed by Zr-CAA. The percentage of chromium removal reached equilibrium after 80 min for the proposed material Zr-CAA with the maximum absorption efficiency up to 85%, whereas for AA, the equilibrium was achieved after 60 min with maximum absorption efficiency up to 58%. This indicates the adsorption of chromium for Zr-CAA occurred in two consecutive steps, where the first one was found to be fastest, in which the transfer of chromium ions from the aqueous phase to the external surface of Zr-CAA was higher. Moreover, the second one was slower, where the diffusion of chromium ions between the Zr-CAA bundles was slower. Furthermore, Fig. 11 demonstrates the effect of solution temperature on the adsorption process of chromium ions via Zr-CAA and AA adsorbent materials. This study includes four different temperatures, that is, 283, 293, 308, and 323 K under constant shaking time. It was observed that increasing the solution temperature from 283 to 323 K was associated with a significant increase in the percentage of chromium(VI) removal by Zr-CAA (Fig. 11). These findings confirmed the endothermic behavior of this adsorption process.

3.2.4. Effect of common ion

The effect of the ionic force over the absorption Cr(VI) ions is one of the significant parameters influencing the absorption process of adsorbent material in the aqueous solution. This effect creates multiple states of absorption in which the interaction between the surfaces of Zr-CAA and chromium ions is either gravitational or non-catalytic. Fig. 12 suggests that the ionic strength with different concentrations of potassium nitrate impairs the absorption process of chromium ions. The increase in the concentration of potassium nitrate in the testing solution leads to the decrease of ionic strength due to the abundance of cationic ions (K^+), which reduces the absorption of chromium ions onto the surface of the Zr-CAA and AA. This happens due to the abundance of charge on the surface of the used material [36]. The interference experiment was carried out with some metals such as Bi^{+2}, Cu^{+2}, Mg^{+2}, Fe^{+2}, and Pb^{+2}. The experimental results suggested that the interference was found minimal and did not exceed (2%–4%) the efficiency of removing Cr(VI) except iron. However, for iron, the interference rate was high and reached up to 35%, so the interference was treated by adding a solution of sodium fluoride to block the effect of the iron metal as per Fig. 13, hence, the efficiency of removing the Cr(VI) became excellent [36].

3.3. Kinetic properties of Cr(VI) sorption onto Zr-CAA and AA

Several kinetic models can be used to describe the kinetics of adsorption. In the present work, different common

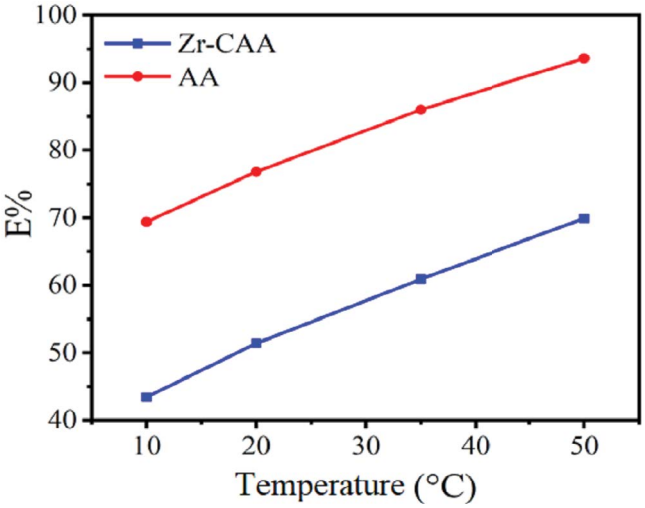

Fig. 11. Effect of temperature on the sorption percentage of Cr(VI) by Zr-CAA and AA from aqueous media at 283, 293, 308, and 323 K.

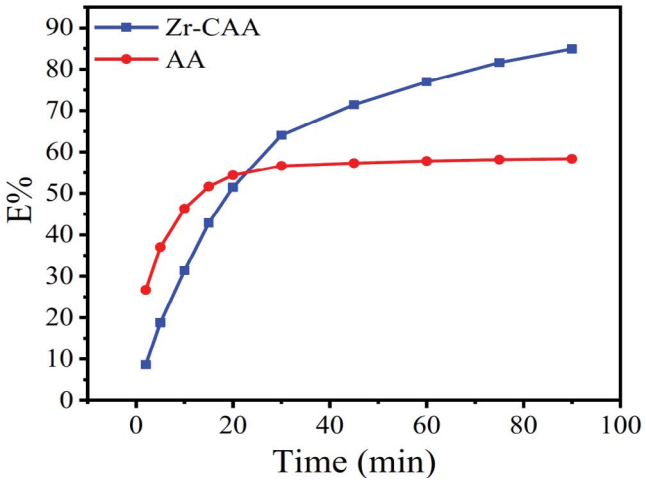

Fig. 10. Effect of shaking time on the absorption of Cr(VI) by Zr-CAA and AA at 25°C ± 3°C from aqueous media.

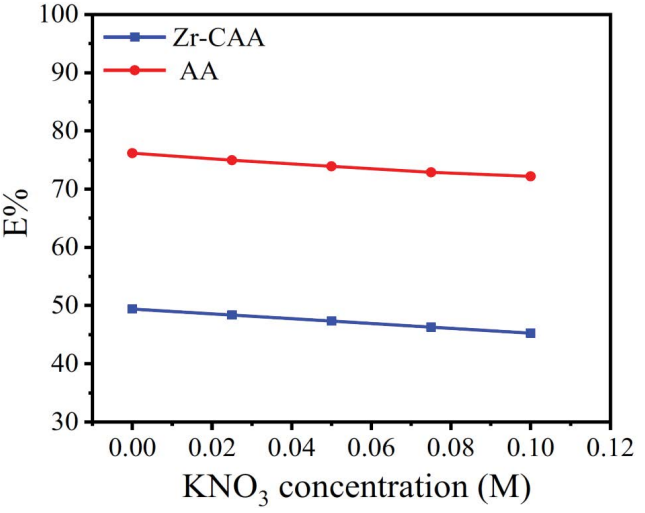

Fig. 12. Effect of KNO_3 on the adsorption percentage of Cr(VI) by Zr-CAA and AA from aqueous media at 20°C.

equations were analyzed to find the best-fitted model for the experimental data obtained, namely pseudo-first-order, pseudo-second-order model, Lagergren plot, fractional power model plots, Weber–Morris model, Elovich, and intra-particle diffusion models.

In this section, the Kinetics for the absorption of Cr(VI) ions from the aqueous media by Zr-CAA and AA were carried out. This analysis demonstrates many indications such as the direction of the reaction, time of completion, and shaking effect, etc. Moreover, the obtained results were supported by calculating the half-life time to absorb the ions from the aqueous phase on the Zr-CAA. The values obtained against the time ($t_{1/2}$) required to absorb the chromium on the surface of Zr-CAA were calculated from the plots of $\log C/C_0$ vs. time for chromium(VI) sorption onto Zr-CAA. The value of $t_{1/2}$ was found to be 1.8 ± 0.07 min in agreement with the values of $t_{1/2}$ reported earlier. Thus, the kinetics of chromium(VI) adsorption onto the Zr-CAA depended on intra-particle diffusion, where the faster one dominates the overall transport rate. The absorbed chromium(VI) onto Zr-CAA was based on the Weber–Morris model [37]:

$$q_t = R_d (t)^{1/2} \quad (1)$$

where R_d is representing the rate constant of intra-particles transport and q_t defines the adsorbed concentration of Cr(VI) at t time. The plot of q_t vs. time can be clearly shown in Fig. 11. The values of R_d determined from the two secret slopes of the Weber–Morris plots (Fig. 14), for the Zr-CAA equal 0.93 and 0.35 mg g^{-1}, with correlation coefficient (R^2 = 0.998) and (R^2 = 0.991), respectively; AA were found equal, 0.62 and 0.06 mg g^{-1}, with correlation coefficient (R^2 = 0.982) and (R^2 = 0.975), respectively.

The fractional power function kinetic model, which was refitted from the Freundlich equation, can be showed by the following:

$$\ln q_t = \ln a + b \ln t \quad (2)$$

where q_t (mg g^{-1}) represents the concentration of chromium(VI) ions adsorbed per unit mass at time t of Zr-CAA, while a and b show coefficients with $b < 1$. Applying the equation of fractional power function to the experimental data of the adsorption process is shown in Fig. 15. The data come together well with the correlation coefficient value R^2 = 0.8803 and 0.96 for Zr-CAA and AA, respectively. The different kinetic models, parameters, and data for Zr-CAA and AA solid phases, are presented in Table 1. This data indicates that the fractional power function kinetic model was not suitable for the absorption of chromium(VI) ions by Zr-CAA and AA.

Among the equations in which a different degree of absorption of chromium ion's is measured, the absorption

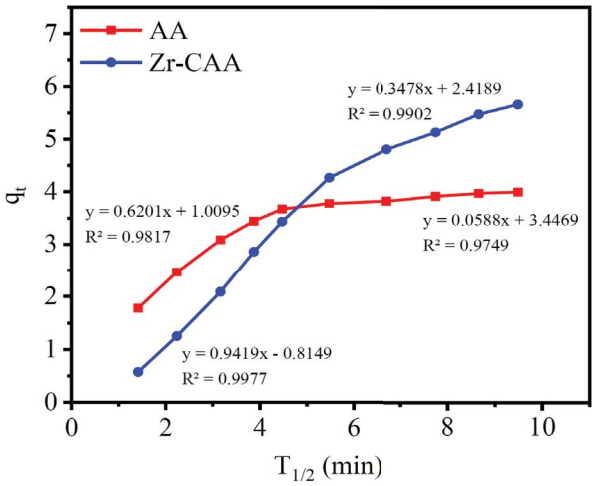

Fig. 14. Weber–Morris plot of chromium(VI) absorption by Zr-CAA vs. square root of time.

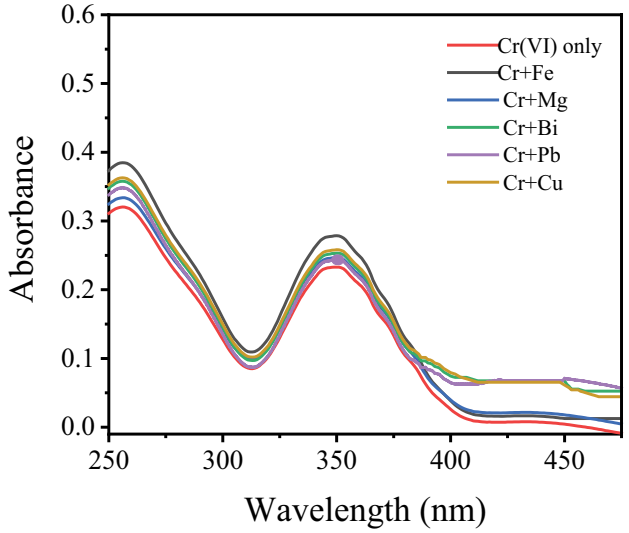

Fig. 13. Effect of many cationic on adsorption of Cr(VI) in aqueous phase.

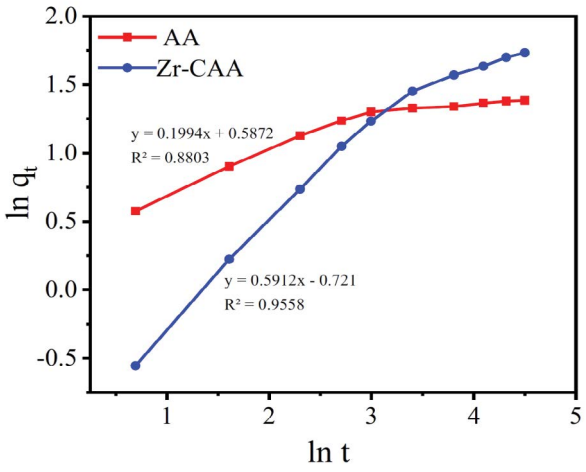

Fig. 15. Fractional power model plots of chromium(VI) by Zr-CAA and AA. (Experimental conditions: 10 mL solution, pH = 1, shaking time = 120 min, temperature = 308 K, chromium concentration 20 mg L^{-1}, and 50 mg of Zr-CAA).

rates in the liquid phase are demonstrated by the Lagergren equation [38,39]:

$$\log\left(q_e - q_t\right) = \log q_e - \frac{k_{\text{Lager}} \times t}{2.303} \quad (3)$$

where, q_e is the concentration of Cr(VI) absorbed at equilibrium per unit mass of the used sorbent; K_{Lager} is the first-order rate constant for the retention process, and t is time. The plot of $\log(q_e - q_t)$ vs. time was linear, where the calculated values of K_{Lager} and q_e were found equal to 0.042 min^{-1} and 4.7 mg g^{-1} for the Zr-CAA, respectively, with the correlation coefficient R^2 = 0.99 (Fig. 16). On the other hand, for AA, these values were found equal to 0.053 min^{-1} and 1.45 mg g^{-1}, respectively, with a correlation coefficient R^2 = 0.96 (Fig. 16). Furthermore, the obtained data were not confirmed in the first-order kinetics of the sorption of Cr(VI) species onto the used solid sorbent.

The pseudo-second-order equation has also been interpreted as a special kind of Langmuir kinetics [40,41], by assuming the following: the adsorbate concentration is constant with time; the total number of binding sites depends on the amount of adsorbate at equilibrium. The linearized form of pseudo-second-order rate was expressed by the following equation:

$$\frac{t}{q_t} = \frac{1}{h} + \left(\frac{1}{q_e}\right)t \quad (4)$$

where $h = k_2 q_e^2$ can be demonstrated as the original sorption percentage, while q_e and q_t are the concentration adsorbed per unit mass over stability at any time. In these positions, the plots of t/q_t vs. t can be shown as linear as demonstrated in Fig. 17. The second-order rate constant (k_2) and equilibrium capacity (q_e) for ions were calculated from the slope that intercepts the Zr-CAA was found equal to 6.1 × 10^{-3} g (mg min)$^{-1}$ and 7.14 mg g^{-1}, respectively, with excellent correlation (R^2 = 0.999). On the other hand, for AA, it was found equal to 8.01 × 10^{-2} g (mg min)$^{-1}$ and 4.12 mg g^{-1}, respectively, with excellent correlation (R^2 = 0.999). The pseudo-second-order kinetic model is the most appropriate one to describe the adsorption of chromium ions by Zr-CAA from an aqueous solution where the values of the pseudo-second-order rate constant k_2 frequently depend on the experimental environments like metal concentration, solution pH, and temperature [42–44].

To express the adsorption capacity of the adsorbed material, an Elovich model was applied, which has significance in the interpretation or repair of chemical kinetics and heterogeneous surfaces. This model is compatible

Table 1
Different kinetic models parameters for the adsorption of chromium(VI) on the Zr-CAA at 293 K

Fractional power function kinetic model				
	A	b	ab	R^2
AA	1.8	0.2	0.36	0.881
Zr-CAA	2.06	0.591	1.21	0.956
Pseudo-first-order kinetic (Lagregen) model				
	$q_{e,\text{exp}}$ (mg g^{-1})	$q_{e,\text{calc}}$(mg g^{-1})	k_1	R^2
AA	3.99	1.45	0.053	0.961
Zr-CAA	5.66	4.7	0.042	0.991
Pseudo-second-order kinetic model				
	$q_{e,\text{exp}}$ (mg g^{-1})	$q_{e,\text{calc}}$(mg g^{-1})	k_2	R^2
AA	5.66	7.14	8.1 × 10^{-2}	0.999
Zr-CAA	5.66	7.14	6.1 × 10^{-3}	0.999
Elovich kinetic model				
	α (g mg^{-1} min^{-1})	β (mg g^{-1} min^{-1})		R^2
AA	12.67	0.677		0.962
Zr-CAA	1.234	1.652		0.957

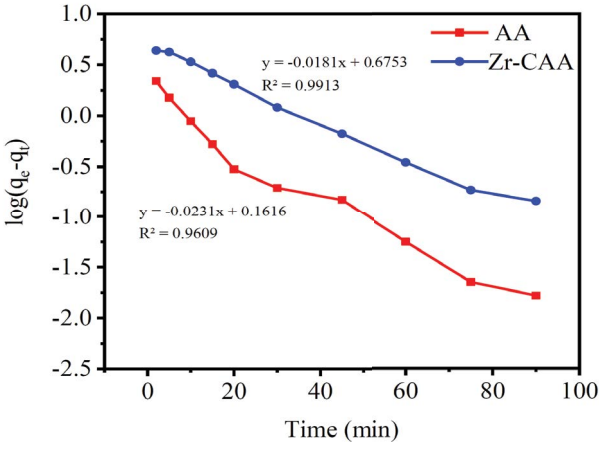

Fig. 16. Lagergren plot of chromium(VI) absorbed by Zr-CAA and AA vs. time. Experimental conditions are mentioned in the batch extraction step.

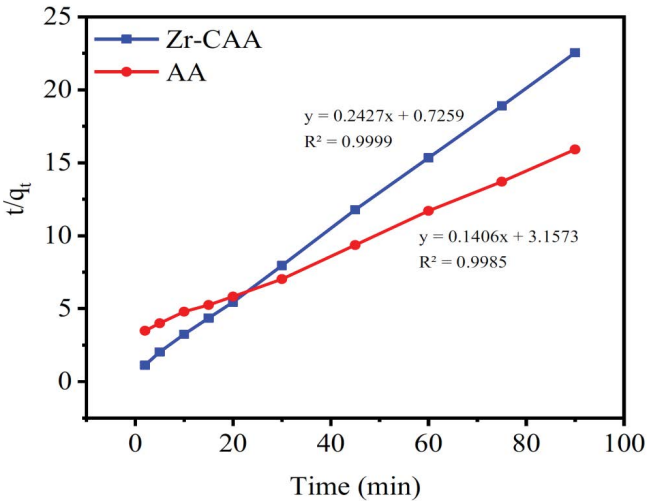

Fig. 17. Pseudo-second-order plot of chromium(VI) uptake by Zr-CAA and AA vs. time. Experimental conditions are mentioned in the batch extraction step.

with such studies that can be expressed with the following equation:

$$q_t = \beta \ln(\alpha\beta) + \beta \ln t \quad (5)$$

where α (g(mg min)$^{-1}$) is the original adsorption percentage and β (g(mg min)$^{-1}$) is the desorption coefficient. The plot of q_t vs. ln$t$ was linear (Fig. 18). The Elovich conditions α and β were calculated from the intercepts and the slopes of Fig. 18. For chromium(VI) ions, the values were found equal to 1.23 g (mg min)$^{-1}$ and 1.65 g (mg min)$^{-1}$, respectively; (R^2 = 0.958) was adsorbed onto Zr-CAA and found equal to 12.67 g (mg min)$^{-1}$ and 0.677 g (mg min)$^{-1}$, respectively; (R^2 = 0.962) adsorbed onto AA. This was based on the obtained results used in the absorption field from the kinetic models of heavy metal ions and the pseudo model Elovich from the first degree and the pseudo-model from the second degree, by looking at the correlation values. It can be concluded that the most appropriate model to describe the absorption of chromium ions is the second model.

3.4. Thermodynamic properties of Cr(VI) retention onto Zr-CAA

The sorption of chromium(VI) onto Zr-CAA over a wide temperature range (293–323 K) was important to find out the chromium(VI) retention onto Zr-CAA. The thermodynamic condition (ΔG, ΔH, and ΔS) express the following [40]:

$$\ln K_c = \frac{-\Delta H}{RT} + \frac{\Delta S}{R} \quad (6)$$

$$\Delta G = \Delta H - T\Delta S \quad (7)$$

$$\Delta G = -RT \ln K_c \quad (8)$$

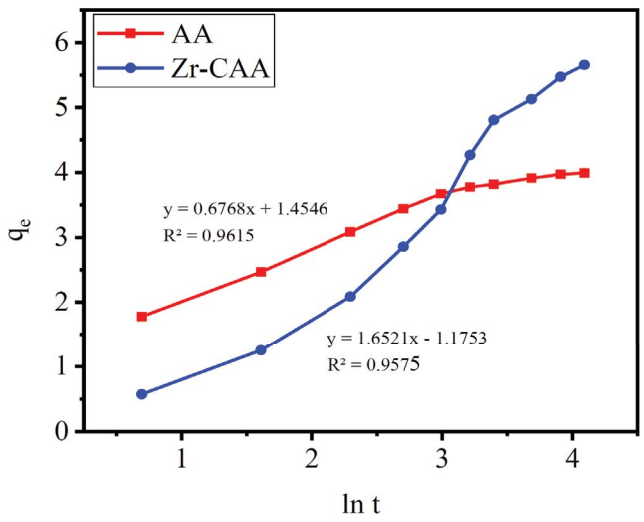

Fig. 18. Elovich model plot for chromium(VI) uptake by Zr-CAA and AA vs. time. Experimental conditions are mentioned in the batch extraction step.

where ΔG, ΔH, and ΔS are the Gibbs free energy, entropy, and enthalpy changes, respectively. R is the gas constant (≈8.314 J K^{-1} mol^{-1}), T is the temperature in Kelvin, and K_c is the equilibrium constant depending on the fractional attainment (F_e) of the sorption. The values of K_c for retention of chromium(VI) ions from the aqueous media at equilibrium onto the solid sorbent were determined by employing the given equation:

$$K_c = \frac{F_e}{1 - F_e} \quad (9)$$

The plot of lnK_c vs. 1,000/T for chromium(VI) retention onto Zr-CAA was linear as seen in Fig. 19 at the temperatures ranging from 293 to 323 K. The equilibrium constant increased with the increased temperature, revealing that the retention of chromium(VI) ions onto the used sorbents is an endothermic process. The numerical values of ΔG, ΔH, and ΔS for chromium(VI) ions were retention determined from the slope and the interception of the linear plot of lnK_c vs. 1,000/T (Fig. 16): –20.78 ± 0.6 kJ mol^{-1}, 71.42 ± 0.4 J mol^{-1} K^{-1}, and –41.7 ± 0.2 kJ mol^{-1} (at 293 K), respectively, for AA; –35.13 ± 0.5 kJ mol^{-1}, 130.3 ± 0.7 J mol^{-1} K^{-1}, and –73.3 ± 0.3 kJ mol^{-1} (at 293 K), respectively, for Zr-CAA.

The ΔH value reveals the endothermic behavior of the uptake process and reflects the difference in bond energy between the sorbent and the analyte. The value of entropy for Zr-CAA suggested the increase in the degree of freedom at the liquid–solid interface, mostly encountered in chromium ions binding due to the release of water molecules of the hydration sphere during the adsorption processes. The negative Gibb's free energy at 293 K for the fabricated Zr-CAA attributes the spontaneous sorption nature of chromium retention onto Zr-CAA.

3.5. Environmental applications

To demonstrate the applicability of the fabricated Zr-CAA adsorbent material, different test samples were prepared from three different water samples collected from

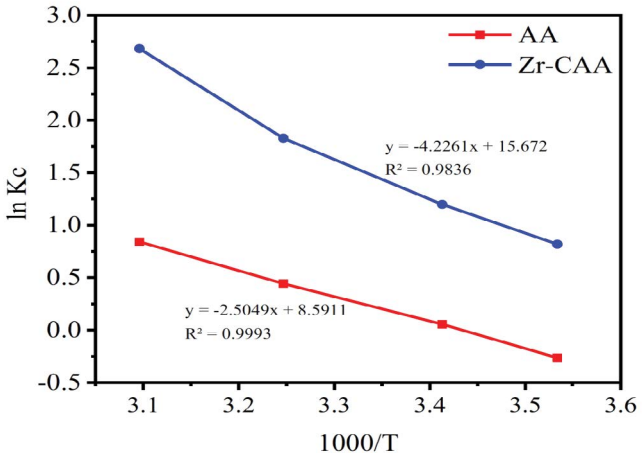

Fig. 19. Plot of lnK_c of chromium(VI) sorption from aqueous media by Zr-CAA vs. 1,000/T.

Table 2
Comparison of Zr-CAA adsorbent with the other reported composite adsorbents

Samples	Initial concentration (mg L^{-1})	Adsorption capacity (mg g^{-1})	Temperature (K)	pH	Ref.
Chitosan-stabilized nanostructured iron oxide	5	1.74	398	5.5	[45]
Agricultural waste biomass	50	2.13	298	4.4	[46]
Corn stalk based anion exchanger	100	2	298	2	[47]
Crystalline magnetite (Magh) nanoparticles	50	7.3	298	2	[48]
Clay	10	0.2	313	2.5	[49]
Palygorskite	100	58.48	298	7	[44]
Riverbed	7.84	0.15	308	2.5	[50]
Volcanic pumice	10	0.046	298	2	[51]
VB	5	0.792	298	2	[52]
Silica sand coated with groundwater treatment residuals	10	6.49	398	7	[53]
Zr-CAA	20	7.14	298	1	This work

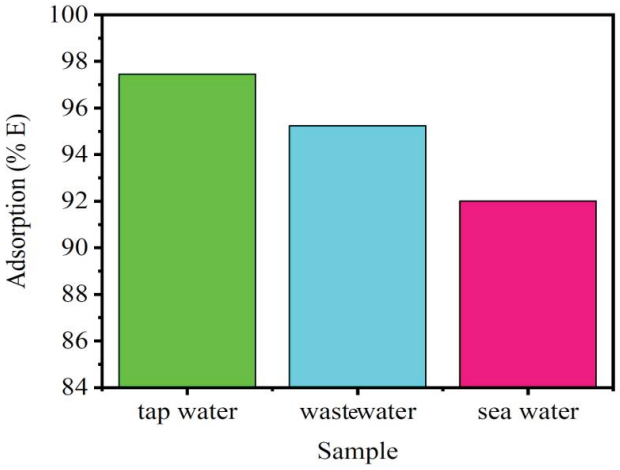

Fig. 20. Removal percentages of chromium ions from different real samples by formed Zr-CAA (experimental conditions: 10 mL solution, pH = 1, shaking time = 120 min, temperature = 308 K, chromium concentration 20 mg L^{-1}, and 50 mg of Zr-CAA).

the tap, sewage, and seawater. After that, predetermined chromium ions were applied to the previous solutions with a concentration of 20 mg L^{-1} and an appropriate amount of the adsorbed (50 mg) substance was added. After setting the pH of approximately 1, the solutions were shaken for 2 h under the temperature of 308 K. The obtained results showed that the adsorption of chromium samples was 92.01% for the Red Sea water, 95.23% for the wastewater, and 97.45 for tap water when the samples were spiked with 20 mg L^{-1} of chromium(VI) ions (Fig. 20). Subsequently, the used Zr-CAA was washed with acetone, dried, and reused for the extraction of Cr(VI) from the solution. Almost the same ratio of adsorption was obtained for all three water samples. These results proved the ability of Zr-CAA to be reused for several adsorption cycles without losing adsorption efficiency. Table 2 shows the comparison of the adsorption efficiency of Zr-CAA toward Cr(VI) concerning the other reported composite adsorbents.

4. Conclusion

This study reported the fabrication of Zr(IV) coordinated CAA adsorbent material and its utilization as a selective adsorbent for Cr(VI) removal from aqueous media. The fabrication of Zr-CAA adsorbent material was investigated by various instrumental analyses such as FT-IR, FE-SEM, EDX, and XRD that confirm the successful coordination of Zr(IV) with CAA. The chromium sorption capacity of fabricated Zr-CAA adsorbent material achieved up to 7.14 mg g^{-1} within 60 min. It was concluded that the solution pH highly influenced the sorption of chromium(VI) at pH 1–2. Moreover, optimum environments were found at the original Cr(VI) concentration of 20 mg L^{-1}, Zr-CAA dosage of 20 mg, the temperature of 293 K for 40 mL of the reaction volume for efficient biosorption. The thermodynamic parameters revealed that the nature of Cr(VI) adsorption was endothermic and spontaneous. The kinetics of a reaction followed the pseudo-second-order model and intra-particle diffusion pattern. The presence of other anions Bi^{+2}, Cu^{+2}, Mg^{+2}, Fe^{+2}, and Pb^{+2} had no significant effect on the adsorption of Cr(VI) except Fe^{+2}. The mechanism of Cr(VI) removal by the fabricated Zr-CAA adsorbent material was supposed to follow the surface complexation and electrostatic attraction. The experimental results demonstrate that the toxic Cr(VI) can be easily and economically separated from different types of aqueous media using the proposed Zr-CAA. This method has the characteristics of high efficiency and low cost to dispose of sludge.

Acknowledgments

Taif University Researchers Supporting Project number (TURSP-2020/244), Taif University, Taif, Saudi Arabia.

References

[1] S. Hanif, A. Shahzad, Removal of chromium(VI) and dye Alizarin Red S (ARS) using polymer-coated iron oxide (Fe_3O_4) magnetic nanoparticles by co-precipitation method, J. Nanopart. Res.,16 (2014) 1–15.

[2] M. Naushad, G. Sharma, A. Kumar, S. Sharma, A. Ghfar, A.A. Bhatnagar, F.J. Stadler, M.R. Khan, Efficient removal of toxic phosphate anions from aqueous environment using pectin based quaternary amino anion exchanger, Int. J. Biol. Macromol., 106 (2018) 1–10.
[3] H.J. Gibb, P.S. Lees, P.F. Pinsky, B.C. Rooney, Lung cancer among workers in chromium chemical production, Am. J. Ind. Med., 38 (2000) 115–126.
[4] F. Fu, Q. Wang, Removal of heavy metal ions from wastewaters: a review, J. Environ. Manage., 92 (2011) 407–418.
[5] M.L. Zheng, K. Fujita, W.Q. Chen, X.M. Duan, S. Kawata, Two-photon excited fluorescence and second-harmonic generation of the DAST organic nanocrystals, J. Phys. Chem. C, 115 (2011) 8988–8993.
[6] R.S. Dongre, K.K. Sadasivuni, K. Deshmukh, A. Mehta, S. Basu, J.S. Meshram, M.A.A.A. Maadeed, A. Karim, Natural polymer based composite membranes for water purification: a review, Polym. Plast. Technol. Eng., 58 (2019) 1295–1310.
[7] G. Sharma, D. Pathania, M. Naushad, N. Kothiyal, Fabrication, characterization and antimicrobial activity of polyaniline Th(IV) tungstomolybdophosphate nanocomposite material: efficient removal of toxic metal ions from water, Chem. Eng. Technol., 251 (2014) 413–421.
[8] O. Kusku, B.L. Rivas, B.F. Urbano, M. Arda, N. Kabay, M. Bryjak, A comparative study of removal of Cr(VI) by ion exchange resins bearing quaternary ammonium groups, J. Chem. Technol. Biotechnol.,89 (2014) 851–857.
[9] A. Özer, H. Altundoğan, M. Erdem, F. Tümen, A study on the Cr(VI) removal from aqueous solutions by steel wool, Environ. Pollut., 97 (1997) 107–112.
[10] R. Epsztein, E. Shaulsky, N. Dizge, D.M. Warsinger, M. Elimelech, Role of ionic charge density in Donnan exclusion of monovalent anions by nanofiltration, Environ. Sci. Technol., 52 (2018) 4108–4116.
[11] Y. Li, J. Qiu, Y. Wang, H. Zhang, Novel iron-decorated carbon nanorods from fullerene soot, Chem. Commun., 6 (2004) 656–657.
[12] Y. Xiaolin, T. Shengrui, G. Maofa, Adsorption of heavy metal ions from aqueous solution by carboxylated cellulose nanocrystals, J. Environ. Sci., 25 (2013) 933–943.
[13] V. Tomar, D. Kumar, A critical study on efficiency of different materials for fluoride removal from aqueous media, Chem. Cent. J., 7 (2013) 1–15.
[14] L.S. Zhong, J.S. Hu, H.P. Liang, A.M. Cao, W.G. Song, L.J. Wan, Self-assembled 3D flowerlike iron oxide nanostructures and their application in water treatment, J. Adv. Mater., 18 (2006) 2426–2431.
[15] S. Asuha, X. Zhou, S. Zhao, Adsorption of methyl orange and Cr(VI) on mesoporous TiO_2 prepared by hydrothermal method, J. Hazard. Mater., 181 (2010) 204–210.
[16] C. Jeon, J.Y. Park, Y.J. Yoo, Characteristics of metal removal using carboxylated alginic acid, Water Res., 36 (2002) 1814–1824.
[17] Y.C. Lin, S.L. Wang, Chromium(VI) reactions of polysaccharide biopolymers, Chem. Eng. Technol., 181 (2012) 479–485.
[18] G. Sewvandi, S. Adikary, Removal of heavy metals from wastewater using chitosan, Manage. Syst. Int. J., 66 (2011) 1–6.
[19] J. Zevallos, A.T. Labbé, A theoretical analysis of the Kohn-Sham and Hartree-Fock orbitals and their use in the determination of electronic properties, J. Chil. Chem. Soc., 48 (2003) 39–47.
[20] C. Jeon, J.Y. Park, Y.J. Yoo, Removal of heavy metals in plating wastewater using carboxylated alginic acid, Korean J. Chem. Eng., 18 (2001) 955–960.
[21] B.C. Son, K. Park, S.H. Song, Y.J. Yoo, Selective biosorption of mixed heavy metal ions using polysaccharides, Korean J. Chem. Eng., 21 (2004) 1168–1172.
[22] N. Viswanathan, S. Meenakshi, Enhanced and selective fluoride sorption on Ce(III) encapsulated chitosan polymeric, J. Appl. Polym. Sci., 112 (2009) 1114–1121.
[23] M. Rajaonarivony, C. Vauthier, G. Couarraze, F. Puisieux, P. Couvreur, Development of a new drug carrier made from alginate, J. Pharm. Sci., 82 (1993) 912–917.
[24] J. Wang, Nanomaterial-based electrochemical biosensors, Analyst, 130 (2005) 421–426.
[25] Z. Marczenko, Separation and Spectrophotometric Determination of Elements, New York NY, 1986.
[26] F. Wang, Z.S. Liu, H. Yang, Y.X. Tan, J. Zhang, Hybrid zeolitic imidazolate frameworks with catalytically active TO_4 building blocks, Angew. Chem. Int. Ed., 123 (2011) 470–473.
[27] S. Gadipelli, W. Travis, W. Zhou, Z. Guo, A thermally derived and optimized structure from ZIF-8 with giant enhancement in CO_2 uptake, Energy Environ. Sci., 7 (2014) 2232–2238.
[28] Y. Hu, H. Kazemian, S. Rohani, Y. Huang, Y. Song, *In situ* high pressure study of ZIF-8 by FTIR spectroscopy, Chem. Commun., 47 (2011) 12694–12696.
[29] S. Luanwuthi, A. Krittayavathananon, P. Srimuk, M. Sawangphruk, *In situ* synthesis of permselective zeolitic imidazolate framework-8/graphene oxide composites: rotating disk electrode and Langmuir adsorption isotherm, RSC Adv., 5 (2015) 46617–46623.
[30] D.K. Panchariya, R.K. Rai, E.A. Kumar, S.K. Singh, Core–shell zeolitic imidazolate frameworks for enhanced hydrogen storage, ACS Omega, 3 (2018) 167–175.
[31] H. Paudyal, B. Pangeni, K. Inoue, H. Kawakita, K. Ohto, K.N. Ghimire, S. Alam, Preparation of novel alginate based anion exchanger from *Ulva japonica* and its application for the removal of trace concentrations of fluoride from water, Bioresour. Technol.,148 (2013) 221–227.
[32] D. Zhou, L. Zhang, S. Guo, Mechanisms of lead biosorption on cellulose/chitin beads, Water Res., 39 (2005) 3755–3762.
[33] X. Zhao, Q. Li, X. Ma, Z. Xiong, F. Quan, Y. Xia, Alginate fibers embedded with silver nanoparticles as efficient catalysts for reduction of 4-nitrophenol, RSC Adv., 5 (2015) 49534–49540.
[34] Y. Su, H. Cui, Q. Li, S. Gao, J.K. Shang, Strong adsorption of phosphate by amorphous zirconium oxide nanoparticles, Water Res., 47 (2013) 5018–5026.
[35] Z.M.M. Balcerzak, Separation, Preconcentration and Spectrophotometry in Inorganic Analysis, Elsevier Science, Warsaw, 2000.
[36] Z. Reddad, C. Gerente, Y. Andres, Pierre Le Cloirec, Environ. Sci. Technol., 36 (2002) 2067–2073.
[37] L.P. Ding, S.K. Bhatia, F. Liu, Kinetics of adsorption on activated carbon: application of heterogeneous vacancy solution theory, Chem. Eng. Sci., 57 (2002) 3909–3928.
[38] B. Bayat, Combined removal of zinc(II) and cadmium(II) from aqueous solutions by adsorption onto high-calcium Turkish fly ash, Water Air Soil Pollut., 136 (2002) 69–92.
[39] G. Sharma, M. Naushad, Adsorptive removal of noxious cadmium ions from aqueous medium using activated carbon/zirconium oxide composite: isotherm and kinetic modelling, J. Mol. Liq., 310 (2020) 113025 (1–6), doi: 10.1016/j.molliq.2020.113025.
[40] M.A. Abdel-Fadeel, H.M. Al-Saidi, A.A. El-Bindary, A.Z. El-Sonbati, S.S. Alharthi, Cloud point extraction – Microvolume spectrophotometry for extraction and determination of bismuth in waters and roadside soil, J. Mol. Liq., 249 (2018) 963–969.
[41] G. Sharma, M. Naushad, AH. Al-Muhtaseb, A. Kumar, M.R. Khan, S. Kalia, Fabrication and characterization of chitosan-crosslinked-poly(alginic acid) nanohydrogel for adsorptive removal of Cr(VI) metal ion from aqueous medium, Int. J. Biol. Macromol., 95 (2017) 484–493.
[42] T. Braun, J.D. Navratil, A.B. Farag, Polyurethane Foam Sorbents in Separation Science, CRC Press, Boca Raton FL, 1985.
[43] A.K. Tabrez, V.S. Ved, Removal of cadmium(II), lead(II), and chromium(VI) ions from aqueous solution using Cl, Toxicol. Environ. Chem., 8 (2010) 1435–1446.
[44] J.H. Potgieter, S.P. Vermaak, P.D. Kalibantonga, Heavy metals removal from solution by palygorskite clay, Miner. Eng., 5 (2006) 463–470.
[45] P.M.B. Chagas, L.B.D. Carvalho, A.A. Caetano, F.G.E. Nogueira, A.D. Corrêa, I.R. Guimarães, Nanostructured iron oxides stabilized by chitosan: using copper to enhance degradation by a combined mechanism, J. Environ. Chem. Eng., 6 (2018) 1008–1019.
[46] U.K. Garg, M.P. Kaur, V.K. Garg, D. Sud, Removal of hexavalent chromium from aqueous solution by agricultural waste biomass, J. Hazard. Mater., 140 (2007) 60–68.

[47] W. Cao, Z. Wang, H. Ao, B. Yuan, Removal of Cr(VI) by corn stalk based anion exchanger: the extent and rate of Cr(VI) reduction as side reaction, Colloids Surf., A, 539 (2018) 424–432.
[48] L.B. Tahar, M.H. Oueslati, M.J.A. Abualreish, Synthesis of magnetite derivatives nanoparticles and their application for the removal of chromium(VI) from aqueous solutions, J. Colloid Interface Sci., 512 (2018) 115–126.
[49] T.A. Khan, V.V. Singh, Removal of cadmium(II), lead(II), and chromium(VI) ions from aqueous solution using clay, Toxicol. Environ. Chem., 92 (2010) 1435–1446.
[50] Y. Sharma, C. Weng, Removal of chromium(VI) from water and wastewater by using riverbed sand: kinetic and equilibrium studies, J. Hazard. Mater., 142 (2007) 449–454.
[51] E. Alemayehu, S.T. Bruhn, B. Lennartz, Adsorption behavior of Cr(VI) onto macro and micro-vesicular volcanic rocks from water, Sep. Purif. Technol., 78 (2011) 55–61.
[52] A. Alemu, B. Lemma, N. Gabbiye, M.T. Alula, M.T. Desta, Removal of chromium(VI) from aqueous solution using vesicular basalt: a potential low cost wastewater treatment system, Heliyon, 4 (2018) e00682 (1–22), doi: 10.1016/j.heliyon.2018.e00682.
[53] C.C. Kan, A.H. Ibe, K.K.P. Rivera, R.O. Arazo, M.D.G. de Luna, Hexavalent chromium removal from aqueous solution by adsorbents synthesized from groundwater treatment residuals, Sustainable Environ. Res., 27 (2017) 163–171.